

Article

Application of Variable-Order Fractional Calculus to the Modeling of Calendar Aging in Lithium-Ion Batteries

Juan Antonio López-Villanueva ^{1,*} , Pablo Rodríguez-Iturriaga ² , Luis Parrilla ² , Salvador Rodríguez-Bolívar ¹ ¹ Department of Electronics and Computer Technology, CITIC, 18071 Granada, Spain² Department of Electronics and Computer Technology, 18071 Granada, Spain

* Correspondence: jalopez@ugr.es

Abstract: Battery aging is one of the key challenges that electrochemical energy storage faces. Models for both cycling and calendar aging are valuable for quantitatively assessing their contribution to overall capacity loss. Since batteries are stored and employed under varying conditions of temperature and state of charge in their real-life operation, the availability of a suitable model to anticipate the outcome of calendar aging in lithium-ion batteries under dynamic conditions is of great interest. In this article, we extend a novel model to predict the capacity loss due to calendar aging by using variable-order fractional calculus. For this purpose, some theoretical difficulties posed by variable-order definitions are discussed and compared by applying them to fit experimental results with a multi-parameter optimization procedure. We show that employing a variable-order model allows for a significant improvement in accuracy and predictive ability with respect to its constant-order counterpart. We conclude that variable-order models constitute an interesting alternative for reproducing complex behavior in dynamical systems, such as aging in lithium-ion batteries.

Keywords: Li-ion battery; calendar aging; fractional calculus; variable order



Citation: López-Villanueva, J.A.; Rodríguez-Iturriaga, P.; Parrilla, L.; Rodríguez-Bolívar, S. Application of Variable-Order Fractional Calculus to the Modeling of Calendar Aging in Lithium-Ion Batteries. *Energies* **2023**, *16*, 2484. <https://doi.org/10.3390/en16052484>

Academic Editor: Quanqing Yu

Received: 20 January 2023

Revised: 28 February 2023

Accepted: 1 March 2023

Published: 5 March 2023



Copyright: © 2023 by the authors. Licensee MDPI, Basel, Switzerland. This article is an open access article distributed under the terms and conditions of the Creative Commons Attribution (CC BY) license (<https://creativecommons.org/licenses/by/4.0/>).

1. Introduction

Rechargeable lithium-ion batteries are regarded as the leading technology for electrochemical energy storage [1,2], and their pre-eminence is expected to increase in the coming years due to the improvement in performance and the forecasted decrease in costs [3]. Despite the important advances achieved in recent years, the battery long-term health is still a major concern and remains a key research topic [4–7]. There is plenty of experimental evidence that the performance of lithium-ion batteries fades not only as a result of charging and discharging, which is referred to as cycle aging [8,9], but also when they are stored with no applied current for long periods of time, which is known as calendar aging [5,10,11]. Although both aging types are relevant and require extensive research, this article is focused on calendar aging. Furthermore, it may also be superimposed to the capacity loss associated with cycled operation when electric current is applied [12].

Calendar aging is usually investigated by storing the battery cell inside a thermal chamber at a chosen ambient temperature and also setting a specific state of charge. Its main effects are a reduction in the remaining usable capacity, as well as an increase in internal resistance [5]. The temperature and state of charge are thus kept constant except for short periods, in which variations in capacity and resistance are measured. In many experiments, a set of battery cells is studied under several combinations of these parameters in order to obtain their functional dependence on them so as to quantitatively determine their influence [13–15]. In some pioneering papers, Broussely et al. [16] observed a quadratic dependence of storage time on capacity loss for different Li-ion battery chemistries, whereas Bloom et al. [11] showed that the area-specific impedance and power fade data followed a general Arrhenius equation proportional to the square root of time. Many authors have also observed a similar power-law dependence with an exponent equal to or similar to 0.5 [11,13,15,17–23], while other authors proposed an exponent in the region of

0.75 [14,24–26], so there is no unambiguous agreement on the value of this parameter. This power-law relationship is multiplied by a factor dependent on the state of charge and temperature, and several semiempirical models have been used with some free parameters, which, despite having a physical justification [27], are usually determined by fitting to experimental data [9,13,17–19]. The temperature dependence is often assumed to follow an Arrhenius-based semiempirical model [14], although other dependencies have also been proposed [12,22]. However, in normal operation, a battery works under dynamic conditions with a variable state of charge and temperature [5,21], and various models have been developed to predict the calendar aging of Li-ion batteries under these varying storage conditions [10,13,17–19,28–32]. Even during cycled operation, calendar aging processes may also take place, and, as a result, cycle and calendar aging are coupled. In order to quantify the contribution of each mechanism to total cell degradation, the effect of calendar aging can be subtracted from overall aging and the pure cycling effects can be analyzed [13], but this requires modeling calendar aging under said dynamic conditions [17–19,29]. We have recently proposed a model based on fractional calculus for this purpose [32].

The main idea behind the model presented in [32] is that many of the systems exhibiting experimental power-law behaviors are typically described by fractional-order models [33,34], so that the similarity between power-law behavior and fractional-order models has motivated the frequent association between them [35]. Hence, the power law dependence with time observed in calendar aging results can be the solution of a fractional order differential equation as well, in a similar way to other applications related to the modeling of fatigue or damage [36]. One example is the creep or time-dependent deformation of rocks under a load lower than their short-term strength [37]. Calendar aging is thus a novel application of fractional calculus. Nevertheless, fractional-order models have already been used in battery modeling, mainly to represent the electrical behavior of battery cells, the relating voltage and the current both in the frequency and time domains [38–40]. The non-integer behavior has been unequivocally observed in electrochemical impedance spectroscopy (EIS) measurements [38,41], in which the frequency response of the cell is characterized. Fractional-order equivalent circuit models also lead to fractional-order differential equations that can be solved in the time domain [42,43], being specially cautious about the correct initialization since the result of fractional-order differential equations depends on the complete history of the system [44]. To aid in this task, we have recently proposed a computationally efficient approximation to the fractional-order circuit element known as the ZARC [45], and have used it to develop a novel dual fractional-order extended Kalman filter for an improved estimation of the battery state of charge [46]. However, in the novel application of fractional calculus proposed in [32], it is not the electrical magnitude but the battery capacity loss due to aging which obeys a fractional-order differential equation. The model obtained this way was applicable under dynamic storage conditions observed in real-life operation, provided higher accuracy than previous semiempirical models, and was also able to reproduce the non-monotonic behavior that is observed when the state of charge or temperature are changed considerably.

However, despite the advantageous performance of the calendar aging model in [32], it can be improved by extending it to a variable-order model. The previous model assumed a constant-order behavior, but the order exponent that provided a good agreement with the experimental capacity loss for short storage times was different from the optimal order exponent obtained for long storage periods, which suggested that the order exponent should vary with time itself. This idea has also been applied to other contexts in which the constant-order fractional models were not able to address some types of physical phenomena, and the order exponent itself is a function of either dependent or independent variables [47]. This is the case for mechanical fatigue or fracture in which variable-order fractional models showed a satisfactory behavior [48,49]. Mathematically, variable-order fractional calculus was proposed as an extension of its constant-order counterpart [50]. A detailed analysis and some useful definitions were provided in [51], which we will use to propose an extended model for capacity loss due to calendar aging in this paper, so

that the prediction capability of the model reported in ref. [32] may be enhanced. This is the main contribution of this article, in which we review a recent model that represents a novelty in the battery aging literature in itself, and extend and improve it, also discussing its predictive capability.

The outline of this article is as follows. Section 2 briefly reviews the fundamentals of variable-order fractional calculus and extends the constant-order fractional model for calendar aging under dynamic conditions to the case of variable order. The final model, dependent on five parameters, as well as the optimization procedure used to determine said parameters, is described in Section 3. The application of this method to a dataset of experimental results is detailed in Section 4. The parameter values obtained in the optimization processes are discussed in Section 5, and finally some conclusions are drawn in Section 6.

2. Fractional-Order Calendar Aging Model under Dynamic Conditions

2.1. Constant-Order Model

In this subsection, we review the fractional-order model proposed in [32] to predict the capacity loss of a battery cell under dynamic conditions. The starting point was the widely employed power-law dependence of the capacity loss [11,13–15,18,20,21,24]

$$L(t) = K(SOC, T) \cdot t^z, \tag{1}$$

with the capacity loss, $L(t)$, defined as

$$L(t) = \frac{Q_0 - Q(t)}{Q_0}, \tag{2}$$

where $Q(t)$ is the capacity at time t and Q_0 is the initial capacity. Function $K(SOC, T)$ depends on the state of charge, SOC, and the temperature, T. It is assumed to be a constant in the time interval $(0, t)$.

By using fractional calculus, we observed that the power-law dependence of the capacity loss $L(t)$ given in (1), is the solution of Equation (3) below [42,43]

$$\frac{d^z L(t)}{dt^z} = \Gamma(z + 1)K(SOC, T), \tag{3}$$

where $\Gamma(z)$ is the well-known Gamma function [43].

We proposed to generalize Equation (3) to a case in which function K is not constant. For this purpose, we assumed that the SOC and T dependence of function $K(SOC, T)$, which had been experimentally determined under static conditions, could also be used under dynamic conditions, when the state of charge and the temperature are changed. Time was then discretized in a series of subintervals $[0, t_1], (t_1, t_2], (t_2, t_3], \dots, (t_{k-1}, t_k]$, and the function $K(SOC, T)$ was approximated by a constant value within each subinterval, with values $K_1, K_2, K_3, \dots, K_k$, respectively. Equation (3) was then integrated by using the Riemann–Liouville definition of the fractional integral of order z , $D^{-z}f(t)$ [43], given in Equation (4).

$$D^{-z}f(t) = \frac{1}{\Gamma(z)} \int_0^t \frac{f(\tau)}{(t - \tau)^{1-z}} d\tau. \tag{4}$$

The result is

$$L(t) = z \int_0^t \frac{K[SOC(\tau), T(\tau)]}{(t - \tau)^{1-z}} d\tau, \tag{5}$$

where the relationship

$$\frac{\Gamma(z + 1)}{\Gamma(z)} = z, \tag{6}$$

has been used.

By subdividing the interval $[0, t_k]$ into its subintervals, and using the value of K in each of them, the result at time t_k is

$$L(t_k) = z \sum_{j=1}^k K_j \int_{t_{j-1}}^{t_j} \frac{d\tau}{(t_k - \tau)^{1-z}}, \tag{7}$$

and the result for the fractional-order model is given in (8).

$$L(t_k) = \sum_{j=1}^k K_j [(t_k - t_{j-1})^z - (t_k - t_j)^z]. \tag{8}$$

Equation (8) summarizes the main result of our previous model in ref. [32], where we demonstrated that it produces a qualitative improvement over previous models for calendar aging under dynamic conditions [17,19]. A remarkable feature of (8) is that it is not necessarily monotonic, since the last time instant, t_k , appears in all the terms. Therefore, the complete history of storage conditions have an influence on capacity loss, thus incorporating into the model the memory behavior that is characteristic of fractional calculus. This is a qualitative advantage over previous models, which were not able to predict the non-monotonic behavior. However, we have observed that the quantitative accuracy can be further improved by extending the model to variable order. This augmented model reported in this article is a novel result and will be detailed in the rest of this section.

2.2. Variable-Order Fractional Calculus

Variable-order fractional calculus was proposed as an extension of its constant-order counterpart [50]. A detailed analysis and some useful definitions were provided in [51]. Definitions of fractional derivatives used in this article start from the Riemann–Liouville fractional integral of order z , defined in [42,43], which were extended to variable order in [51]. In that work, the derivative of order $-z(t)$, or equivalently the integral of order $z(t)$, was defined as

$${}_0d_t^{-z(t)} f(t) = \int_0^t \frac{(t - \tau)^{z(t,\tau)-1}}{\Gamma[z(t, \tau)]} f(\tau) d\tau. \tag{9}$$

Lorenzo et al. [51] distinguished several special cases of Equation (9):

- Case no memory of order

$${}_0d_t^{-z(t)} f(t) = \frac{1}{\Gamma[z(t)]} \int_0^t (t - \tau)^{z(t)-1} f(\tau) d\tau \tag{10}$$

- Case memory of order

$${}_0d_t^{-z(t)} f(t) = \int_0^t \frac{(t - \tau)^{z(\tau)-1}}{\Gamma[z(\tau)]} f(\tau) d\tau \tag{11}$$

or

$${}_0d_t^{-z(t)} f(t) = \int_0^t \frac{(t - \tau)^{z(t-\tau)-1}}{\Gamma[z(t - \tau)]} f(\tau) d\tau \tag{12}$$

Lorenzo et al. [51] also considered the case in which the order exponent is generalized to any function $z[(S(t))]$. However, we only consider in this article the case in which the exponent depends explicitly on time, $S(t) = t$, since it is enough to achieve a remarkable improvement in the degree of agreement with the experimental results, as we will show in the next section.

We now discuss the consequences of the variable order in the static case, in which a constant value is assumed for function $K(SOC, T)$ in the time interval $(0, t)$, and we will discuss the dynamic case in the next subsection.

In the case of no memory of order, Equation (10) provides a result similar to (4), so that

$$L(t) = K(SOC, T) \cdot t^{z(t)}. \tag{13}$$

To illustrate the effect of the time dependence of the order exponent, we assumed the simplest case of a linear function:

$$z(t) = z_0 + d_z t, \tag{14}$$

The results for different choices of d_z are shown in Figure 1. z_0 is adjusted to reach the same capacity loss in the four curves after a storage period of one year. The time dependence of the order exponent becomes apparent in the difference in curvature.

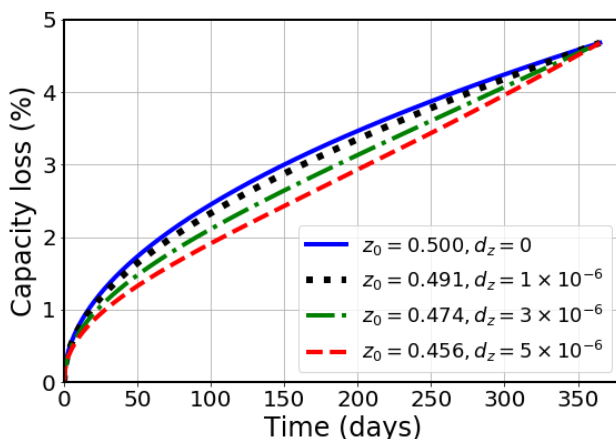


Figure 1. Capacity loss versus time for four different values of d_z , expressed in h^{-1} . z_0 is adjusted to reach the same capacity loss after one year of storage. $K = 5 \times 10^{-4}$, with time expressed in hours.

When the order exponent $z(t)$ is not constant, the dimensions of the coefficient $K(SOC, T)$ become an issue [52]. To avoid this, a reference time can be selected so that K is dimensionless and the capacity loss is defined as:

$$L(t) = K(SOC, T) \cdot \left(\frac{t}{t_{ref}} \right)^{z(t)}, \tag{15}$$

where t_{ref} is the employed time unit. However, if $K(SOC, T)$ does not depend explicitly on time with one choice of unit of time, it will if another time unit is chosen. For example, with the linear dependence of the exponent given in Equation (14):

$$L(t) = K_h(SOC, T) \cdot \left(\frac{t}{1 \text{ hour}} \right)^{z_{01} + d_{z1}(t)}, \tag{16}$$

with t expressed in hours, or:

$$L(t) = K_d(SOC, T) \cdot (24)^{z_{01} + d_{z1}(t)} \cdot \left(\frac{t}{1 \text{ day}} \right)^{z_{01} + d_{z1}(t)}, \tag{17}$$

with t expressed in days. The additional time dependence can lead to modified parameter values

$$L(t) = K_d(SOC, T) \cdot \left(\frac{t}{1 \text{ day}} \right)^{z_{02} + d_{z2}(t)} \tag{18}$$

Consequently, if $K_h(SOC, T)$ does not depend on time, $K_d(SOC, T)$ does, or an effective constant $K_d(SOC, T)$ may be chosen with a different exponent.

The effect of time units is shown in Figure 2. Curves corresponding to Equations (16) and (18) closely match each other but the time dependence, $z(t)$, is different in the two cases. We have chosen $K_h = 3 \times 10^{-4}$, $z_{01} = 0.5$, and $d_{z1} = 5.42 \times 10^{-6} \text{ h}^{-1}$ in Equation (16) to obtain a capacity loss of 10% after two years, and have fitted the parameter values to obtain a good agreement with Equation (18), obtaining $K_d = 1.506 \times 10^{-3}$, $z_{02} = 0.5$, and $d_{z2} = 1.88 \times 10^{-4} \text{ day}^{-1}$. The curves obtained by choosing $z_{02} = z_{01}$ and $d_{z2} = d_{z1}$ are also shown for comparison in two cases, with $K_d = K_h \cdot (24)^{z_{01}}$ and $K_d = K_h \cdot (24)^{z_{max}}$, with $z_{max} = z_{01} + d_z t_{max}$, respectively. According to this discussion, we have chosen $t_{ref} = 1 \text{ h}$ in calculations in this paper, and will omit it explicitly in most expressions, although we will use t in *days* as the unit in the horizontal axis of graphs for better visibility.

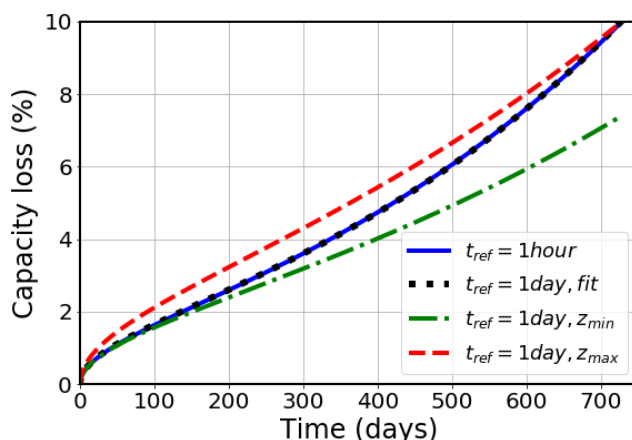


Figure 2. Capacity loss versus time for Equations (16) with $K_h = 3 \times 10^{-4}$, $z_{01} = 0.5$, and $d_{z1} = 5.42 \times 10^{-6} \text{ h}^{-1}$, and (18) with $K_d = 1.506 \times 10^{-3}$, $z_{02} = 0.5$, and $d_{z2} = 1.88 \times 10^{-4} \text{ day}^{-1}$. Curves with $K_d = K_h \cdot (24)^{z_{min}}$ and $K_d = K_h \cdot (24)^{z_{max}}$, being $z_{min} = z_{01}$ and $z_{max} = z_{01} + d_z t_{max}$, respectively, are shown for comparison.

2.3. Variable-Order Model

In this subsection, we extend the model detailed in Section 2.1 to the case of variable order defined in Section 2.2 by introducing the time dependence of exponent z directly in the discretized result (8).

To use Equations (10)–(12) under dynamic conditions, we discretized time in a series of subintervals, and we approximated the function $K(SOC, T)$ by a series of constant values $K_1, K_2, K_3, \dots, K_k$, respectively, as in ref [32]. Hence, in the case of no memory of order, at the end of k th interval, Equation (10) becomes

$$L(t_k) = z(t_k) \sum_{j=1}^k K_j \int_{t_{j-1}}^{t_j} (t_k - \tau)^{z(t_k)-1} d\tau, \tag{19}$$

giving a result for the variable-order fractional model similar to (8), but with exponents dependent on time, as follows

$$L(t_k) = \sum_{j=1}^k K_j \left[(t_k - t_{j-1})^{z(t_k)} - (t_k - t_j)^{z(t_k)} \right]. \tag{20}$$

We consider now the case of memory of order. As mentioned in the previous section, instead of directly using Equations (11) or (12) that extend the Riemann–Liouville integral,

which are much more computationally expensive to apply, we extended the integrated result (8), obtaining analogous results to Equation (20). The corresponding equations are

$$L(t_k) = \sum_{j=1}^k K_j \left[(t_k - t_{j-1})^{z(t_{j-1})} - (t_k - t_j)^{z(t_j)} \right], \tag{21}$$

and

$$L(t_k) = \sum_{j=1}^k K_j \left[(t_k - t_{j-1})^{z(t_k - t_{j-1})} - (t_k - t_j)^{z(t_k - t_j)} \right], \tag{22}$$

respectively.

The three resulting equations, namely (20), (21), and (22), will be compared to experimental results below.

3. Validation Method

In order to complete the model and be able to compare the variable-order results with experimental data in the general case of dynamic conditions, we had to choose a form for the function $K(SOC, T)$. This function can be factored as a product of two terms, one of them dependent on temperature and the other expressed as a function of state of charge. A Tafel-type function was chosen to write the state-of-charge dependence in terms of the cell potential [13,15,19], while an Arrhenius-type dependence was assumed for the temperature term. [11,20].

For this purpose, we have chosen the model used by Schimpe et al. [13], given in (23).

$$K(SOC, T) = k_{Ref} \exp\left(\frac{\alpha F(U_{a,ref} - U_a)}{R_g T_{ref}}\right) \exp\left(-\frac{E_a}{R_g} \left(\frac{1}{T} - \frac{1}{T_{ref}}\right)\right), \tag{23}$$

where $R_g = 8.314 \text{ J}/(\text{mol} \cdot \text{K})$ is the universal gas constant and $F = 96485.3 \text{ C}/\text{mol}$ is the Faraday constant. U_a is the anode voltage, taken from Safari et al. [53]. The reference potential $U_{a,ref}$ is set to $U_a(SOC = 50\%) = 0.123 \text{ V}$ and $T_{ref} = 298.15 \text{ K}$.

This function of SOC and T was obtained for static conditions, but we assumed that it can also be used when the state of charge and the temperature change, as also assumed by several authors [13,17,18,29,30]. To fit the experimental results under these dynamic conditions, we left three free parameters: the scale factor k_{ref} , parameter α for the SOC dependence, and the activation energy, E_a , for the temperature dependence. Furthermore, to apply the variable-order model, the simple linear dependence of the order exponent on time given in Equation (14) was assumed. Therefore, in addition to the three parameters of the semiempirical $K(SOC, T)$ model, we had two additional parameters, z_0 and d_z . The complete final model thus depends on five parameters ($k_{ref}, \alpha, E_a, z_0, d_z$) that can be determined by a multiparametric optimization procedure.

To find the optimal values of said five parameters, we used the nature-inspired metaheuristic Cuckoo search algorithm [54,55]. This procedure has been shown to be simple and perform similar to and even better than other metaheuristic algorithms [56]. This metaheuristic method is based on the brood parasitism of some cuckoo species. Some of its advantages are that it requires one single internal parameter, p_a , defined as the fraction of worse solutions which are abandoned in each iteration, and being enhanced by the Lévy flights rather than by simple isotropic random walks. This algorithm has already been used with a different purpose in the context of fractional-order circuits [57], and we have chosen it as a suitable option for our optimization goal. The pseudo-code of the algorithm [58], applied to a general minimization problem, has been represented as a flowchart in Figure 3. In the context of our specific optimization problem, we have selected a population size of $n = 25$ and a fraction of abandoned nests of $p_a = 0.25$.

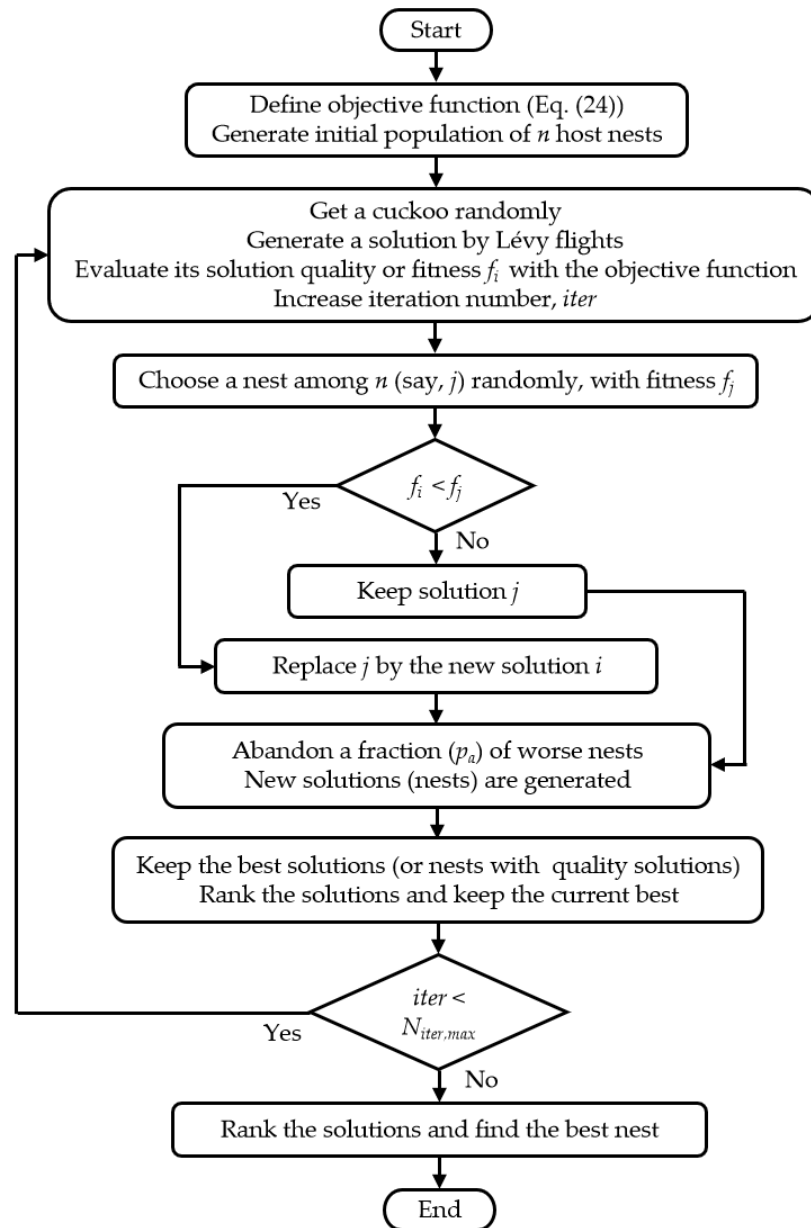


Figure 3. Flowchart for the Cuckoo search algorithm for a minimization problem [58].

The average root mean square error divided by the average of the experimental data values was chosen as the objective function.

$$\overline{\epsilon}_{rms} = \frac{\sqrt{\sum_{j=1}^N [L_j^{(model)} - L_j^{(exp)}]^2}}{\sum_{j=1}^N |L_j^{(exp)}|}, \quad (24)$$

where $L_j^{(model)}$ are the values of capacity loss provided by the model and $L_j^{(exp)}$ are the experimental capacity losses.

Given the expression in Equation (23), the resulting model actually consists of two parts: Equations (20)–(22), which provide a way to account for dynamic conditions and constitute the main contribution of our work, and Equation (23) for the function $K(SOC, T)$, which has been taken from the literature. Analyzing variable-order models for calendar aging in batteries is a challenging task, since long measurement periods are required for

the effects of the varying exponent to be noticeable. There are not many experimental datasets extending for several years with changing storage conditions in the literature, several of which were reviewed in ref. [32]. We tested the full model in that work for different datasets, although with constant a order, observing the high parameter variability that is usual in the literature. Therefore, if data from different cells were taken into account, different parameter values would most likely be obtained in the optimization process. For these reasons, we have selected in this article the dataset that offers the greatest variety of conditions, published by Lucu et al. [6]. This dataset provides the evolution of the remaining capacity of a 20 Ah pouch cell, with a positive electrode of lithium nickel–manganese–cobalt (NMC 4:4:2) and a graphite negative electrode, measured for three years under a wide variety of storage conditions that were changed every month. The state of charge and temperature profiles have been taken from ref. [6] and are shown in Figure 4.

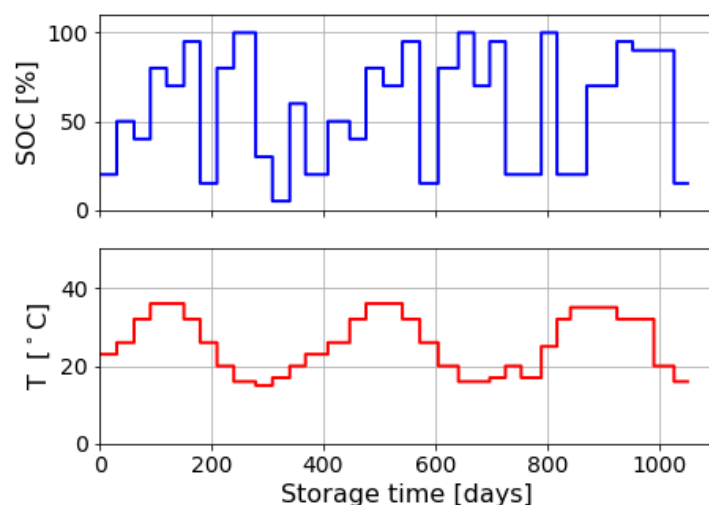


Figure 4. Profiles of SOC and T used in this article to compare the experimental capacity loss produced by calendar aging with the results predicted by our variable-order model. These profiles were used by Lucu et al. and have been reproduced from ref. [6].

The selected experimental data have been used as a whole to obtain the optimal set of model parameters that produces the minimum root-mean-square error. However, in order to demonstrate the predictive ability of the model, the data measured for only a fraction of the storage time has also been employed for parameterization, while the remaining data, with different storage conditions, have been used for validation. The results of these optimization procedures are detailed in Section 4.

4. Comparison with Experimental Results

Equations (20)–(22) have been compared to experimental results. To this end, the set of experimental data described in the previous section was chosen.

The results of the relative capacity with respect to the initial capacity $((1 - L(t)) \times 100)$ are shown in Figure 5 for the cases of constant order and variable order, together with the experimental results. The modeled curve for the constant order case shows a higher error than the curve for the variable-order curve, as expected since we have introduced an additional parameter, and the relative error for the initial points is high in the constant order case, while the result for the variable-order model is quite good despite the high variability in the experimental data. The parameter values obtained in the optimization are shown in Table 1. Different values for the activation energy are obtained in the constant order and the variable order cases. Although we do not have a priori information about the value of this parameter, the result obtained in the variable order case is closer to the value obtained by Schimpe et al. [13] ($E_a = 20,592$ J/mol). However, this issue will be discussed in more detail in Section 5.

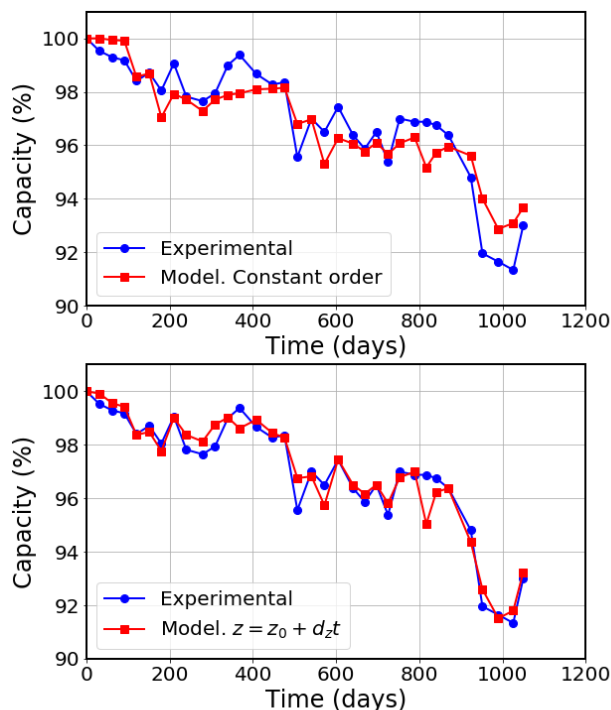


Figure 5. Experimental results from Lucu et al. [6] for capacity, and approximations obtained with the fractional-order model in the cases of constant order (**top**) and variable order (**bottom**).

Table 1. Parameter values for the best agreement with the experimental results of Lucu et al. [6], with a linearly time-dependent order.

Order	k_{ref}	α	E_a [J/mol]	z_0	d_z [h ⁻¹]	ϵ_{rms}
Constant	6.33×10^{-6}	2.181	51,810	0.687	0	5.05%
Variable	5.49×10^{-4}	0.701	29,025	0.300	5.60×10^{-6}	2.94%

We now consider the case of memory of order. As mentioned in the previous section, instead of using Equations (11) or (12) that extend the Riemann–Liouville integral, we extended the integrated result, obtaining Equations (21) and (22). The resulting parameter values are shown in Table 2. Although the root-mean-square error is somewhat higher than in the case of no memory of order, the appearance of the curves is quite similar to those plotted in Figure 5 (bottom), so they are not shown here.

Table 2. Parameter values for the best agreement with the experimental results of Lucu et al. [6], with a linearly time-dependent order in the case of memory of order.

Case	k_{ref}	α	E_a (J/mol)	z_0	d_z (h ⁻¹)	ϵ_{rms}
$z(\tau)$	5.92×10^{-5}	0.0983	10,543	0.658	1.67×10^{-5}	3.21%
$z(t - \tau)$	1.68×10^{-3}	0.989	26,079	0.134	7.09×10^{-6}	3.53%

Finally, the ability of the model to predict long-term aging is analyzed. To do this, the experimental data are fitted with the optimization procedure for a period of time, and then the model with the resulting parameters has been used to predict the capacity loss for the rest of the storage time. The parameter values obtained by fitting the experimental results measured for 541 days (about a year and a half) are used to predict the capacity loss thereafter. The result is shown in Figure 6 and Table 3. As observed, the root-mean-square error increases over time so that if the obtained parameter values are used to predict the

capacity loss up to 725 days (about two years), the error is between 4.8% and 8.3%, while if they are used to predict the whole series of 1050 days (almost three years), the error increases to the range 6.9–12.7%.

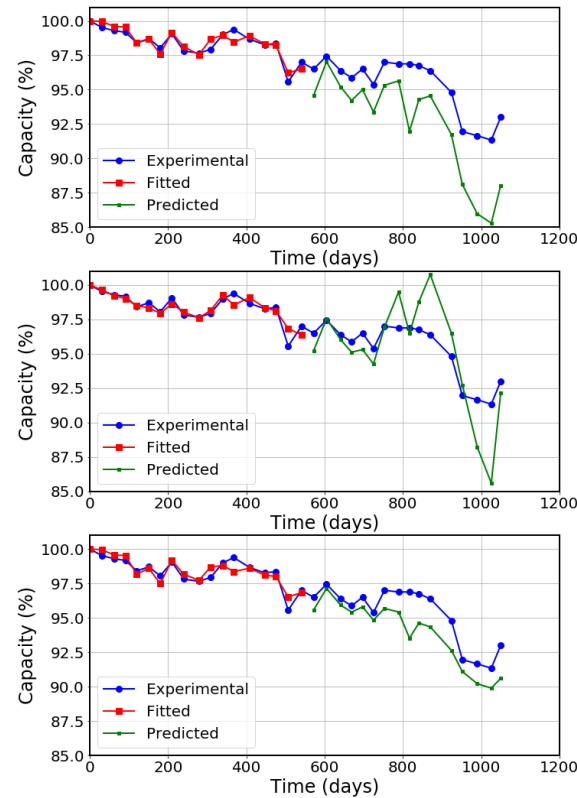


Figure 6. Experimental results from Lucu et al. [6] for capacity, and approximations obtained with the fractional-order model by fitting the experimental results measured in the first 541 days. Prediction is shown for the rest of the storage time. (**top**) $z(t)$, (**middle**) $z(\tau)$, and (**bottom**) $z(t - \tau)$.

Table 3. Parameter values for the best agreement with the experimental results of Lucu et al. [6] for a fit period of 541 days followed by a prediction period.

Case	k_{ref}	α	E_a (J/mol)	z_0	d_z (h^{-1})	ϵ_{rms} (725 Days)	ϵ_{rms} (1050 Days)
$z(t)$	7.59×10^{-4}	0.930	17,037	0.235	8.38×10^{-6}	8.26%	12.7%
$z(\tau)$	2.11×10^{-4}	0.239	51,493	0.508	1.84×10^{-5}	5.84%	9.06%
$z(t - \tau)$	1.45×10^{-3}	0.981	21,675	0.155	8.11×10^{-6}	4.82%	6.49%

Nevertheless, when more data are available, they can be used to improve the prediction capability of the model. As shown in Figure 7 and Table 4, when data from the first 725 days are used to obtain the parameter values, the prediction for the whole data series of 1050 days improves noticeably, resulting in a root-mean-square error of 3.3–3.7%. The best result is also obtained here for the non memory of order case, which reinforces the choice of this definition for the present model, although the memory of order definitions seem to work better in Table 3, so this decision cannot be considered final and analysis of more datasets would be necessary to adopt it.

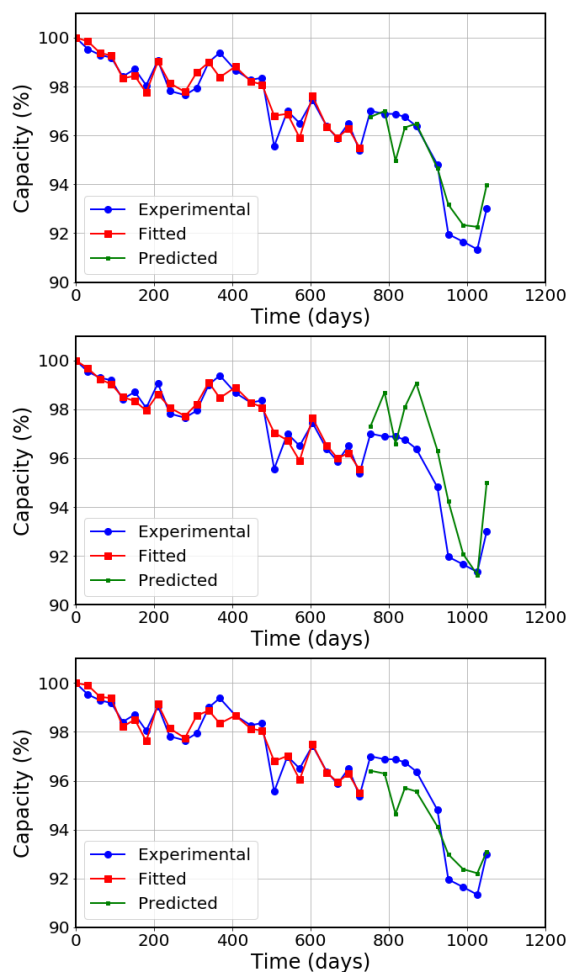


Figure 7. Experimental results from Lucu et al. [6] for capacity, and approximations obtained with the fractional-order model by fitting the experimental results measured in the first 725 days. Prediction is shown for the rest of the storage time. **(top)** $z(t)$, **(middle)** $z(\tau)$, and **(bottom)** $z(t - \tau)$.

Table 4. Parameter values for the best agreement with the experimental results of Lucu et al. [6] for a fit period of 725 days followed by a prediction period.

Case	k_{ref}	α	E_a (J/mol)	z_0	d_z (h^{-1})	ϵ_{rms} (1050 Days)
$z(t)$	9.61×10^{-4}	0.575	15,080	0.268	4.96×10^{-6}	3.30%
$z(\tau)$	2.35×10^{-4}	0.259	7328	0.493	1.390×10^{-5}	5.15%
$z(t - \tau)$	1.61×10^{-3}	0.765	17,152	0.179	6.41×10^{-6}	3.67%

5. Discussion on Results and Limitations

Despite the simple assumption of a linear dependence of the order exponent $z(t)$ with time, a reasonable agreement is achieved between the variable-order fractional model for capacity loss due to calendar aging and the experimental results, both in the cases of memory of order and no memory of order. In spite of this, we can conclude that the memory of order definition shown in Equation (11) should be discarded in this application for the reasons detailed below. First, it is challenging to employ accurately, since the integral in (11) requires costly numerical methods even in the case of a constant K function. In order to achieve the result in (21), we have treated the variable exponent $z(\tau)$ as a constant value within each subinterval (t_{j-1}, t_j) and substituted it by its values at the subinterval extremes. This assumption is not needed with the definition in Equation (10) to obtain Equation (20). Secondly, the parameter values obtained with the optimization procedure, shown in the middle rows of Tables 3 and 4, differ noticeably from those calculated in

the other two cases, and the root-mean-square error is higher in Table 4. Although the error in Table 3 is lower with respect to the non-memory-of-order case (first row), the optimal result provided by the Cuckoo search algorithm shows severe fluctuations in Figures 6 and 7 (middle), while the oscillations in the other two cases are milder. These high fluctuations constitute an additional reason to advise against using the memory of order definition. Given the better predictive ability of the non memory of order case obtained with Equation (20) and shown in the first row of Table 4, we suggest employing it in the application of this model. Although the third case (with the mathematical expression given in Equation (22) and results in the third row of Tables 3 and 4) exhibits a similar degree of accuracy, we still recommend using the non memory of order definition, since Equation (22) is also an approximation to definition (12), similar to that used to solve (11).

Regarding the predictive capability of the model, the results are acceptable, although the error increases over time and the long-term prediction from a limited set of data points is only qualitative. However, when more data are incorporated into the optimization, the prediction capability increases significantly. This is observed in Figure 7 and Table 4, where after using the two-year data series, the prediction for the third year gives satisfactory results, notably in the case of no memory of order, as discussed above.

Another possible limitation is related to the choice of the semiempirical model for function $K(SOC, T)$. We have used Equation (23) that considers the SOC dependence of the negative electrode potential in an exponential function of $\alpha F(U_{a,ref} - U_a)$. A similar dependence was chosen in ref. [19], but other proposals exist in the literature, such as a simple linear dependence [10] or an activation energy in the Arrhenius term dependent on SOC [22]. This work has focused on the applications to dynamic storage conditions, and has not factored in either the underlying physics behind the semi-empirical model or the effect of considering different semiempirical options. Consequently, it is difficult to account for the results provided by optimization procedures based on the exploration of large search spaces such as the Cuckoo search algorithm. An example of this is the variability in parameter α of the SOC-dependent term that has been obtained in the different cases analyzed in Section 4, which has been considered here as a purely empirical parameter. Similar considerations could be made about the other three semi-empirical parameters, k_{ref} , z_0 , and d_z . In fact, the high variation in one parameter may compensate for the differences in the other empirical parameters in order to minimize the error, but justifying the behavior of any of them separately is non-trivial. Activation energy, on the other hand, can be considered to have a more understandable physical meaning. However, there is also no general agreement on this parameter and a wide range of values has been reported in the literature, as shown in Table 5. By applying the different definitions of the variable-order Riemann–Liouville integral, a high dispersion in the activation energy has also been obtained in this article. The non memory of order case provides values between 15,000 and 30,000 J/mol, which are consistent with the value of 20,592 J/mol determined in [13] with the model of $K(SOC, T)$ used here. Furthermore, we have not assumed a dependence of the activation energy on the SOC as proposed by several authors [17,59,60] in order not to increase the number of free parameters.

As a final remark, we should stress that although a semiempirical, physics-based model has been used for $K(SOC, T)$, the model presented here is rather mathematical, and any inquiry into the physical principles of this behavior is outside the scope of this article. However, we encourage researchers to delve into the physical origins of this model, since greater physical insight could guide multi-parameter fitting in such a way that the resulting high variability in the parameters would decrease. Without that knowledge, seemingly different parameter sets could lead to similar-looking results with little difference in the root-mean-square error, with no clear set of criteria to choose between them. Investigation on the physical origin of the several parameters involved in the semiempirical model, and on other alternatives for the $K(SOC, T)$ function, remain open research topics. The validation of the model against other datasets with specifically designed variable storage conditions would also provide additional physical insight. Another pending research task

is to integrate the presented model with models for cycle aging, in order to develop a complete aging model.

Table 5. A selection of activation energy values proposed in the literature.

E_a (kJ/mol)	Positive Electrode	Ref.
50–55 kJ/mol	NCA	[59]
43.6 kJ/mol	NMC	[61]
47–60 kJ/mol	NMC	[8]
52.1 kJ/mol, 182 kJ/mol	LFP	[10]
35.64 kJ/mol	LFP	[21]
58.0 kJ/mol	NMC	[14]
56.94–73.37 kJ/mol	LFP	[17]
52.86 kJ/mol	NCA	[17]
84.88 kJ/mol	LFP	[12]
27.7–28.7 kJ/mol	NMC	[19]
17.13 kJ/mol	LFP	[18]
79.57 kJ/mol	NMC	[12]
20.59 kJ/mol	LFP	[13]
42.7–44.9 kJ/mol	NMC	[60]
36.36 kJ/mol	NMC	[24]

6. Conclusions

In their real-life performance, lithium-ion batteries are stored in the absence of electric current for prolonged periods of time in a variety of conditions of state of charge and temperature, and are thus subjected to calendar aging under dynamic conditions. Even when current is applied, the effects of calendar aging may be superimposed to those of cycle aging, and it is therefore useful to have an accurate model which is valid under these varying conditions. A recent model based on fractional calculus was developed for this purpose, which was able to predict the experimentally observed non-monotonic behavior when the state of charge or the temperature are changed significantly. However, the accuracy of the previous model may be considerably improved if it is extended by including variable order in the fractional order formulation. Variable order requires additional definitions and poses theoretical difficulties that have been discussed in this paper in the context of its application to calendar aging.

The resulting semiempirical model proposed in this article leaves five free parameters to be determined by a multi-parameter fit to the experimental results. A metaheuristic procedure has been used to determine the parameter values that predict the response of a rich experimental dataset available in the literature, and the capability of the model to predict future behavior has also been discussed. Although this model presents an unambiguous advantage, it cannot be considered a finished proposal, and further research is required regarding the availability of new datasets as well as the physical origins of the non-monotonic behavior of calendar aging. Another interesting suggestion for future research is the unification of the proposed calendar model with cycle aging models, aiming to construct a more comprehensive aging model.

Author Contributions: J.A.L.-V., conceptualization, methodology, investigation, writing—original draft, writing—review and editing; P.R.-I., investigation, writing—review and editing; L.P., investigation, writing—review and editing; S.R.-B., methodology, investigation, writing—original draft, writing—review and editing. All authors have read and agreed to the published version of the manuscript.

Funding: This research received no external funding.

Data Availability Statement: No new data were created or analyzed in this study. Data sharing is not applicable to this article.

Conflicts of Interest: The authors declare no conflict of interest.

Nomenclature

Nomenclature employed in this article.

Nomenclature	Description
α	Parameter for the SOC dependence in $K(SOC, T)$ semiempirical model
d_z	Slope of order exponent vs. time
d_a	Fraction of abandoned nests in Cuckoo search algorithm
d_{z1}	Slope of order exponent vs. time with time reference equal to one hour
d_{z2}	Slope of order exponent vs. time with time reference equal to one day
D^{-z}	Riemann–Liouville integral of order z
${}_0d_t^{-z(t)}$	Riemann–Liouville integral with variable order $z(t)$
E_a	Activation energy
$\overline{\epsilon}_{rms}$	Root-mean-square error
f	General function in integral definitions
f_i	Fitness in Cuckoo search algorithm
F	Faraday constant
Γ	Gamma function
k_{ref}	Pre-exponential factor in $K(SOC, T)$ semiempirical model
K	Aging rate, also named stress factor. It is a function of SOC and temperature
K_d	K function with time unit equal to one day
K_h	K function with time unit equal to one hour
K_j	Constant K function within subinterval (t_{j-1}, t_j)
L	Capacity loss
$L_j^{(exp)}$	Experimental capacity loss measured at $t = t_j$
$L_j^{(model)}$	Capacity loss provided by the model at $t = t_j$
n	Number of nests (population size) in Cuckoo search algorithm
Q	Battery cell capacity
Q_0	Capacity of a non-aged cell
R_g	Universal gas constant
SOC	State of charge
t	Time
t_j	Limits of the time subintervals
t_{max}	Maximum time of measurement
t_{ref}	Time reference used as a unit of time for calculation of capacity loss
T	Absolute temperature
T_{ref}	Reference temperature in semiempirical K model
τ	Dummy variable in Riemann–Liouville integrals
U_a	Negative electrode potential as a function of SOC
$U_{a,ref}$	Reference electrode potential in semiempirical K model
z	Order exponent
$z(t)$	Time-dependent order exponent
$z[S(t)]$	Order exponent dependent on an arbitrary function
z_0	Order exponent at time $t = 0$
z_{01}	Order exponent at $t = 0$ with time reference equal to one hour
z_{02}	Order exponent at $t = 0$ with time reference equal to one day
ZARC	Fractional-order circuit element

References

- Zubi, G.; Dufo-López, R.; Carvalho, M.; Pasaoglu, G. The lithium-ion battery: State of the art and future perspectives. *Renew. Sustain. Energy Rev.* **2018**, *89*, 292–308. [[CrossRef](#)]
- Stampatori, D.; Raimondi, P.P.; Noussan, M. Li-Ion Batteries: A Review of a Key Technology for Transport Decarbonization. *Energies* **2020**, *13*, 2638. [[CrossRef](#)]
- Berckmans, G.; Messagie, M.; Smekens, J.; Omar, N.; Vanhaverbeke, L.; Van Mierlo, J. Cost Projection of State of the Art Lithium-Ion Batteries for Electric Vehicles Up to 2030. *Energies* **2017**, *10*, 1314. [[CrossRef](#)]
- Deng, Z.; Hu, X.; Li, P.; Lin, X.; Bian, X. Data-Driven Battery State of Health Estimation Based on Random Partial Charging Data. *IEEE Trans. Power Electron.* **2022**, *37*, 5021–5031. [[CrossRef](#)]

5. Dubarry, M.; Qin, N.; Brooker, P. Calendar aging of commercial Li-ion cells of different chemistries—A review. *Curr. Opin. Electrochem.* **2018**, *9*, 106–113. [[CrossRef](#)]
6. Lucu, M.; Martinez-Laserna, E.; Gandiaga, I.; Liu, K.; Camblong, H.; Widanage, W.; Marco, J. Data-driven nonparametric Li-ion battery ageing model aiming at learning from real operation data—Part A: Storage operation. *J. Energy Storage* **2020**, *30*, 101409. [[CrossRef](#)]
7. Lucu, M.; Martinez-Laserna, E.; Gandiaga, I.; Liu, K.; Camblong, H.; Widanage, W.; Marco, J. Data-driven nonparametric Li-ion battery ageing model aiming at learning from real operation data—Part B: Cycling operation. *J. Energy Storage* **2020**, *30*, 101410. [[CrossRef](#)]
8. Ecker, M.; Nieto, N.; Käbitz, S.; Schmalstieg, J.; Blanke, H.; Warnecke, A.; Sauer, D.U. Calendar and cycle life study of Li(NiMnCo)O₂-based 18650 lithium-ion batteries. *J. Power Sources* **2014**, *248*, 839–851. [[CrossRef](#)]
9. de Hoog, J.; Timmermans, J.M.; Ioan-Stroe, D.; Swierczynski, M.; Jaguemont, J.; Goutam, S.; Omar, N.; Van Mierlo, J.; Van Den Bossche, P. Combined cycling and calendar capacity fade modeling of a Nickel-Manganese-Cobalt Oxide Cell with real-life profile validation. *Appl. Energy* **2017**, *200*, 47–61. [[CrossRef](#)]
10. Grolleau, S.; Delaille, A.; Gualous, H.; Gyan, P.; Revel, R.; Bernard, J.; Redondo-Iglesias, E.; Peter, J. Calendar aging of commercial graphite/LiFePO₄ cell – Predicting capacity fade under time dependent storage conditions. *J. Power Sources* **2014**, *255*, 450–458. . [[CrossRef](#)]
11. Bloom, I.; Cole, B.W.; Sohn, J.J.; Jones, S.A.; Polzin, E.G.; Battaglia, V.S.; Henriksen, G.L.; Motloch, C.; Richardson, R.; Unkelhaeuser, T.; et al. An accelerated calendar and cycle life study of Li-ion cells. *J. Power Sources* **2001**, *101*, 238–247. [[CrossRef](#)]
12. Redondo-Iglesias, E.; Venet, P.; Pelissier, S. Global Model for Self-Discharge and Capacity Fade in Lithium-Ion Batteries Based on the Generalized Eyring Relationship. *IEEE Trans. Veh. Technol.* **2018**, *67*, 104–113. [[CrossRef](#)]
13. Schimpe, M.; von Kuepach, M.E.; Naumann, M.; Hesse, H.C.; Smith, K.; Jossen, A. Comprehensive Modeling of Temperature-Dependent Degradation Mechanisms in Lithium Iron Phosphate Batteries. *J. Electrochem. Soc.* **2018**, *165*, A181–A193. [[CrossRef](#)]
14. Schmalstieg, J.; Käbitz, S.; Ecker, M.; Sauer, D.U. A holistic aging model for Li(NiMnCo)O₂ based 18650 lithium-ion batteries. *J. Power Sources* **2014**, *257*, 325–334. [[CrossRef](#)]
15. Ecker, M.; Gerschler, J.B.; Vogel, J.; Käbitz, S.; Hust, F.; Dechent, P.; Sauer, D.U. Development of a lifetime prediction model for lithium-ion batteries based on extended accelerated aging test data. *J. Power Sources* **2012**, *215*, 248–257. [[CrossRef](#)]
16. Broussely, M.; Herreyre, S.; Biensan, P.; Kasztejna, P.; Nechev, K.; Staniewicz, R. Aging mechanism in Li ion cells and calendar life predictions. *J. Power Sources* **2001**, *97*, 13–21.
17. Petit, M.; Prada, E.; Sauvart-Moynot, V. Development of an empirical aging model for Li-ion batteries and application to assess the impact of Vehicle-to-Grid strategies on battery lifetime. *Appl. Energy* **2016**, *172*, 398–407. [[CrossRef](#)]
18. Naumann, M.; Schimpe, M.; Keil, P.; Hesse, H.C.; Jossen, A. Analysis and modeling of calendar aging of a commercial LiFePO₄/graphite cell. *J. Energy Storage* **2018**, *17*, 153–169. [[CrossRef](#)]
19. Hahn, S.L.; Storch, M.; Swaminathan, R.; Obry, B.; Bandlow, J.; Birke, K.P. Quantitative validation of calendar aging models for lithium-ion batteries. *J. Power Sources* **2018**, *400*, 402–414. [[CrossRef](#)]
20. Wang, J.; Liu, P.; Hicks-Garner, J.; Sherman, E.; Soukiazian, S.; Verbrugge, M.; Tataria, H.; Musser, J.; Finamore, P. Cycle-life model for graphite-LiFePO₄ cells. *J. Power Sources* **2011**, *196*, 3942–3948. [[CrossRef](#)]
21. Sarasketa-Zabala, E.; Gandiaga, I.; Rodriguez-Martinez, L.; Villarreal, I. Calendar ageing analysis of a LiFePO₄/graphite cell with dynamic model validations: Towards realistic lifetime predictions. *J. Power Sources* **2014**, *272*, 45–57. [[CrossRef](#)]
22. Redondo-Iglesias, E.; Venet, P.; Pelissier, S. Eyring acceleration model for predicting calendar ageing of lithium-ion batteries. *J. Energy Storage* **2017**, *13*, 176–183. [[CrossRef](#)]
23. Liu, Y.; Xie, K.; Pan, Y.; Wang, H.; Li, Y.; Zheng, C. Simplified modeling and parameter estimation to predict calendar life of Li-ion batteries. *Solid State Ionics* **2018**, *320*, 126–131. [[CrossRef](#)]
24. Shi, N.; Chen, Z.; Niu, M.; He, Z.; Wang, Y.; Cui, J. State-of-charge estimation for the lithium-ion battery based on adaptive extended Kalman filter using improved parameter identification. *J. Energy Storage* **2022**, *45*, 103518. [[CrossRef](#)]
25. Mathieu, R.; Baghdadi, I.; Briat, O.; Gyan, P.; Vinassa, J.M. D-optimal design of experiments applied to lithium battery for ageing model calibration. *Energy* **2017**, *141*, 2108–2119. [[CrossRef](#)]
26. Gasper, P.; Gering, K.; Dufek, E.; Smith, K. Challenging Practices of Algebraic Battery Life Models through Statistical Validation and Model Identification via Machine-Learning. *J. Electrochem. Soc.* **2021**, *168*, 020502. [[CrossRef](#)]
27. Khaleghi Rahimian, S.; Forouzan, M.M.; Han, S.; Tang, Y. A generalized physics-based calendar life model for Li-ion cells. *Electrochim. Acta* **2020**, *348*, 136343. [[CrossRef](#)]
28. Su, L.; Zhang, J.; Huang, J.; Ge, H.; Li, Z.; Xie, F.; Liaw, B.Y. Path dependence of lithium ion cells aging under storage conditions. *J. Power Sources* **2016**, *315*, 35–46. [[CrossRef](#)]
29. Thomas, E.; Bloom, I.; Christophersen, J.; Battaglia, V. Rate-based degradation modeling of lithium-ion cells. *J. Power Sources* **2012**, *206*, 378–382. [[CrossRef](#)]
30. Mingant, R.; Petit, M.; Belaïd, S.; Bernard, J. Data-driven model development to predict the aging of a Li-ion battery pack in electric vehicles representative conditions. *J. Energy Storage* **2021**, *39*, 102592. [[CrossRef](#)]

31. Lucu, M.; Martinez-Laserna, E.; Gandiaga, I.; Camblong, H. A critical review on self-adaptive Li-ion battery ageing models. *J. Power Sources* **2018**, *401*, 85–101. [[CrossRef](#)]
32. López-Villanueva, J.A.; Iturriaga, P.R.; Rodríguez-Bolívar, S. A fractional-order model for calendar aging with dynamic storage conditions. *J. Energy Storage* **2022**, *50*, 104537. [[CrossRef](#)]
33. Ionescu, C.; Lopes, A.; Copot, D.; Machado, J.; Bates, J. The role of fractional calculus in modeling biological phenomena: A review. *Commun. Nonlinear Sci. Numer. Simul.* **2017**, *51*, 141–159. [[CrossRef](#)]
34. Bonfanti, A.; Kaplan, J.L.; Charras, G.; Kabla, A. Fractional viscoelastic models for power-law materials. *Soft Matter* **2020**, *16*, 6002–6020. [[CrossRef](#)]
35. Sabatier, J. Fractional Order Models Are Doubly Infinite Dimensional Models and thus of Infinite Memory: Consequences on Initialization and Some Solutions. *Symmetry* **2021**, *13*, 1099. [[CrossRef](#)]
36. Wang, M.; Xu, X.; Liu, Q.; Ding, Y.; Shen, F. A nonlinear fractional-order damage model of stress relaxation of net-like red soil. *Sci. Rep.* **2021**, *11*, 22917. [[CrossRef](#)]
37. Zhou, H.; Wang, C.; Han, B.; Duan, Z. A creep constitutive model for salt rock based on fractional derivatives. *Int. J. Rock Mech. Min. Sci.* **2011**, *48*, 116–121. [[CrossRef](#)]
38. Andre, D.; Meiler, M.; Steiner, K.; Walz, H.; Soczka-Guth, T.; Sauer, D.U. A retrospective on lithium-ion batteries. *J. Power Sources* **2011**, *196*, 5349–5356. [[CrossRef](#)]
39. Zou, C.; Zhang, L.; Hu, X.; Wang, Z.; Wik, T.; Pecht, M. A review of fractional-order techniques applied to lithium-ion batteries, lead-acid batteries, and supercapacitors. *J. Power Sources* **2018**, *390*, 286–296. [[CrossRef](#)]
40. Hu, X.; Yuan, H.; Zou, C.; Li, Z.; Zhang, L. Co-Estimation of State of Charge and State of Health for Lithium-Ion Batteries Based on Fractional-Order Calculus. *IEEE Trans. Veh. Technol.* **2018**, *67*, 10319–10329. [[CrossRef](#)]
41. Meddings, N.; Heinrich, M.; Overney, F.; Lee, J.S.; Ruiz, V.; Napolitano, E.; Seitz, S.; Hinds, G.; Raccichini, R.; Gaberšček, M.; et al. Application of electrochemical impedance spectroscopy to commercial Li-ion cells: A review. *J. Power Sources* **2020**, *480*, 228742. [[CrossRef](#)]
42. Podlubny, I. *Fractional Differential Equations: An Introduction to Fraction Derivatives, Fractional Differential Equations, to Methods of Their Solution and Some of Their Applications*; Academic Press: San Diego, CA, USA, 1999; pp. 1–316.
43. Petras, I. *Fractional-Order Nonlinear Systems. Modeling, Analysis and Simulation*; Springer: Berlin/Heidelberg, Germany, 2011.
44. López-Villanueva, J.A.; Rodríguez Bolívar, S. Constant Phase Element in the Time Domain: The Problem of Initialization. *Energies* **2022**, *15*, 792. [[CrossRef](#)]
45. López-Villanueva, J.A.; Rodríguez-Iturriaga, P.; Parrilla, L.; Rodríguez-Bolívar, S. A compact model of the ZARC for circuit simulators in the frequency and time domains. *AEU Int. J. Electron. Commun.* **2022**, 154293. [[CrossRef](#)]
46. Rodríguez-Iturriaga, P.; del Valle, J.A.; Rodríguez-Bolívar, S.; Anseán, D.; Viera, J.C.; López-Villanueva, J.A. A novel Dual Fractional-Order Extended Kalman Filter for the improved estimation of battery state of charge. *J. Energy Storage* **2022**, *56*, 105810. [[CrossRef](#)]
47. Patnaik, S.; Hollkamp, J.P.; Semperlotti, F. Applications of variable-order fractional operators: A review. *Proc. R. Soc. A-Math. Phys. Eng. Sci.* **2020**, *476*, 20190498. [[CrossRef](#)]
48. Wu, F.; Liu, J.F.; Wang, J. An improved Maxwell creep model for rock based on variable-order fractional derivatives. *Environ. Earth Sci.* **2015**, *73*, 6965–6971. [[CrossRef](#)]
49. Patnaik, S.; Semperlotti, F. Variable-order fracture mechanics and its application to dynamic fracture. *NPJ Comput. Mater.* **2021**, *7*, 27. [[CrossRef](#)]
50. Samko, S. Fractional integration and differentiation of variable order: An overview. *Nonlinear Dyn.* **2013**, *71*, 653–662. [[CrossRef](#)]
51. Lorenzo, C.F.; Hartley, T. Variable order and distributed order fractional operators. *Nonlinear Dyn.* **2002**, *29*, 57–98. [[CrossRef](#)]
52. Diethelm, K. A fractional calculus based model for the simulation of an outbreak of dengue fever. *Nonlinear Dyn.* **2013**, *71*, 613–619. [[CrossRef](#)]
53. Safari, M.; Delacourt, C. Modeling of a Commercial Graphite/LiFePO₄ Cell. *J. Electrochem. Soc.* **2011**, *158*, A562. [[CrossRef](#)]
54. Yang, X.S.; Deb, S. Cuckoo Search via Lévy flights. In Proceedings of the 2009 World Congress on Nature Biologically Inspired Computing (NaBIC), Coimbatore, India, 9–11 December 2009; pp. 210–214. [[CrossRef](#)]
55. Yang, X.S.; Deb, S. Engineering optimization by cuckoo search. *Int. J. Math. Model. Numer. Optim.* **2010**, *1*, 330–343.
56. Civicioglu, P.; Besdok, E. A conceptual comparison of the Cuckoo-search, particle swarm optimization, differential evolution and artificial bee colony algorithms. *Artif. Intell. Rev.* **2013**, *39*, 315–346. [[CrossRef](#)]
57. AbdelAty, A.; Fouda, M.E.; Elbarawy, M.T.; Radwan, A. Optimal charging of fractional-order circuits with Cuckoo search. *J. Adv. Res.* **2021**, *32*, 119–131.
58. Yang, X.S. Chapter 9—Cuckoo Search. In *Nature-Inspired Optimization Algorithms*; Yang, X.S., Ed.; Elsevier: Oxford, UK, 2014; pp. 129–139. [[CrossRef](#)]
59. Liaw, B.Y.; Roth, E.; Jungst, R.G.; Nagasubramanian, G.; Case, H.L.; Doughty, D.H. Correlation of Arrhenius behaviors in power and capacity fades with cell impedance and heat generation in cylindrical lithium-ion cells. *J. Power Sources* **2003**, *119*, 874–886.

60. Rumberg, B.; Epding, B.; Stradtman, I.; Schleder, M.; Kwade, A. Holistic calendar aging model parametrization concept for lifetime prediction of graphite/NMC lithium-ion cells. *J. Energy Storage* **2020**, *30*, 101510. [[CrossRef](#)]
61. Käbitz, S.; Gerschler, J.B.; Ecker, M.; Yurdagel, Y.; Emmermacher, B.; André, D.; Mitsch, T.; Sauer, D.U. Cycle and calendar life study of a graphite | $\text{LiNi}_{1/3}\text{Mn}_{1/3}\text{Co}_{1/3}\text{O}_2$ Li-ion high energy system. Part A: Full cell characterization. *J. Power Sources* **2013**, *239*, 572–583. [[CrossRef](#)]

Disclaimer/Publisher's Note: The statements, opinions and data contained in all publications are solely those of the individual author(s) and contributor(s) and not of MDPI and/or the editor(s). MDPI and/or the editor(s) disclaim responsibility for any injury to people or property resulting from any ideas, methods, instructions or products referred to in the content.